# Kinetic Study of the Electrochemical Mineralization of m-Cresol on a Boron-Doped Diamond Anode

Cristina Flox[a, c], Enric Brillas[a], André Savall[b] and Karine Groenen-Serrano[b,*]

[a]*Laboratori d'Electroquímica dels Materials i del Medi Ambient, Departament de Química Física, Facultat de Química, Universitat de Barcelona, Martí i Franquès 1-11, 08028 Barcelona, Spain*

[b]*Laboratoire de Génie Chimique, CNRS, Université Paul Sabatier, 118 route de Narbonne 31062 Toulouse cedex 02, France*

[c]*Catalonia Institute for Energy Research, IREC, Jardins de les Dones de Negre 1, 08930 Sant Adrià de Besòs, (Barcelona), Spain*

**Abstract:** The kinetics of the electrooxidation of *m*-cresol in aqueous solution was investigated in a one-compartment flow electrochemical cell with a boron-doped diamond electrode (BDD). Cyclic voltammograms recorded on BDD revealed that cresol oxidation takes place at a potential very close to the discharge of water. Under potentiostatic conditions, at a working potential lower than water discharge, a passive layer was rapidly formed on the electrode surface due to cresol polymerization. The anode fouling was not observed during electrolysis performed with the flow electrochemical cell operating under galvanostatic conditions. In this case, the decay of *m*-cresol concentration followed a pseudo-first-order kinetics. The abatement of chemical oxygen demand (COD) showed that the kinetics of *m*-cresol oxidation was limited by mass transfer and that a full mineralization was achieved. A good agreement between predicted and experimental COD and instantaneous current efficiency values was obtained, although some deviations were observed at high current since the experimental data decreased faster than those predicted ones. These deviations can be explained by the occurrence of oxygen evolution which increases the mass transfer coefficient.

**Keywords:** Electrooxidation, Boron-doped diamond, Cresol, Wastewater treatment.

## 1. INTRODUCTION

Aromatic compounds are generally toxic and the products having a quinonic structure are characterized by very strong toxicities. Aromatic structures are usually very stable and as a consequence, aqueous effluents polluted with such compounds should be decontaminated by effective physico-chemical techniques of oxidation. Cresols are classified by the US-EPA as persistent, priority and toxic chemicals, showing chronic effects at 12 mg L-1 of the quantitative structure–activity relationship [1]. Unfortunately, the high contamination level that these compounds reach in industrial wastewaters, their seasonal production and the presence of other organic pollutants such as lipids usually render these effluents inappropriate for direct biological treatment. Alternative powerful oxidation technologies are then needed to be developed for achieving total destruction of cresols from wastewaters.

Several papers reported the removal of cresols by advanced oxidation processes (AOPs) [1-4]. The main features of the electrochemical oxidation of cresols on BDD and $PbO_2$ were presented in a previous paper [5]. The use of Fenton's reagent for cresol oxidation is effective during the first steps of the process, but it suffers the formation of by-products like oxalic or acetic acids that limits the mineralization because of the formation of stable complexes with iron ions [6].

Electrochemistry is a convenient technique for the treatment of industrial effluents containing organics. Mineralization of organic compounds can be fully achieved under conditions in which the transfer of oxygen atoms is effective. It is generally assumed that hydroxyl radical (•OH) resulting from water discharge by reaction (1) is particularly active to carry out oxygen atoms transfer [7-10]:

$$H_2O \rightarrow {}^{\bullet}OH + H^+ + e^- \qquad (1)$$

The strong activity of this radical in aqueous solution results from the high value of its standard potential $E^0 = 2.74$ V/SHE [11]. Organic molecules are degraded into smaller molecules by a succession of oxygen atom transfers until complete destruction of the carbon skeleton [10]. In these last 20 years, the use of boron-doped diamond (BDD) has known an increasing interest in the electrochemical community because of its unique properties. BDD produces hydroxyl radicals that are free on its surface and can react massively close to the electrode allowing the complete mineralization of organic compounds.

Several papers reported the rapid removal of *o*-, *m*- and *p*-cresol from waters by electro-oxidation using a BDD anode [5, 12, 13]. The behaviour of BDD was numerically predicted by mathematical model developed by Mascia *et al*. [13] and the effect of the presence of chloride ions on the COD removal was studied.

A previous study [5] showed that the electrochemical incineration of *m*-cresol on a BDD anode occurs by giving by-products in very weak concentration. Furthermore, it was found that the $PbO_2$ anode is comparatively much less efficient due to the lower oxidation ability of hydroxyl radicals that it is able to produce under the same operating conditions.

The aim of this work is to gain a better insight into the kinetics of the electrochemical mineralization of *m*-cresol in a one-compartment flow electrochemical reactor with a BDD anode. The influence of operating parameters such as applied current, initial *m*-cresol concentration and electrolyte flow rate was examined. The results obtained are presented and discussed in terms of *m*-cresol decay, current efficiency and chemical oxygen demand (COD)

*Address correspondence of this author at the Laboratoire de Génie Chimique, CNRS, Université Paul Sabatier, 118 route de Narbonne 31062 Toulouse cedex 02, France; Tel: + 33 (0)5 61 55 86 77; Fax: + 33 (0) 5 61 55 61 39;
E-mail: serrano@chimie.ups-tlse.fr

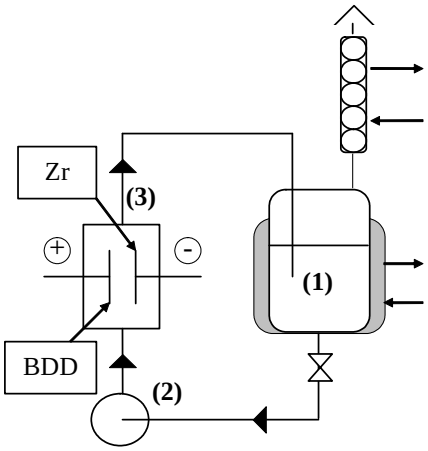


**Fig. (1).** Discontinuous process with a single compartment electrochemical reactor, (1): 1 L tank, (2): centrifugal pump and (3): electrochemical cell.

removal. Cyclic voltammetry was also used to ascertain the nature of the oxidation process as a function of the applied potential.

## 2. EXPERIMENTAL

### 2.1. Chemicals

*m*-Cresol (99% purity) was purchased from Sigma and used as received. Solutions were prepared with high-purity water obtained from a Millipore Milli-Q system (resistivity > 18 MΩ cm at 25 ºC). Analytical grade sulfuric acid from Prolabo was used to adjust the initial pH to 4.0. Anhydrous sodium sulfate employed as supporting electrolyte was analytical grade supplied by Prolabo. Other chemicals and organic solvents were either HPLC or analytical grade from Sigma-Aldrich, Merck and Prolabo.

### 2.2. Cyclic Voltammetric Study

Cyclic voltammograms were carried out in a conventional three-electrode cell of 100 mL capacity using a computer controlled Autolab potentiostat Model 30. A BDD thin film of 0.196 $cm^2$ from Adamant was used as working electrode, a Pt wire as counter electrode and a $Hg/Hg_2Cl_2,Cl^-$(sat) electrode (SME) as the reference electrode. Before each experiment, the electrode was pre-treated using anodic polarisation at 2.84 V/SHE during 40 s into a 1 M $H_2SO_4$ solution.

### 2.3. Electrochemical Reactor

Electrolyses were conducted in a one-compartment flow filter-press reactor under galvanostatic conditions (Fig. **1**) The electrolyte was stored in a 1 liter thermoregulated glass reservoir (1) and circulated through the electrolytic cell using a centrifugal pump (2). Electrodes were two discs of 63 cm² of active surface separated 10 mm. The BDD anode from Adamant was elaborated by chemical vapour deposition on a conductive substrate of silicium. The cathode was a 1 mm thick disc of zirconium. The current was supplied by an ELC AL 924 power supply.

### 2.4. Analysis Procedures

Samples withdrawn from treated solutions were filtered with Whatman 0.45 µm PTFE filters before analysis. The mineralization process was monitored from COD decay. COD was determined by photometry by means of test tubes ready for use and of a pocket photometer (Dr Changes Lasa 50 system).

*m*-Cresol concentration was followed by reversed-phase HPLC chromatography using a Hewlett-Packard 1100 Series liquid chromatograph, fitted with a Spherisorb ODS2 5 µm, 150 mm x 4.6 mm (i.d.), column at room temperature, equipped with an UV/Vis detector selected at λ = 276 nm and controlled with an Agilent ChemStation software. These measurements were made by injecting 20 µL aliquots and circulating a 50:45:5 (v/v/v) methanol/phosphate buffer (pH = 2.5)/pentanol mixture at 1.0 mL $min^{-1}$ as mobile phase.

### 2.5. Kinetic Regimes

The kinetics of the electrode processes can be controlled either by mass transfer or by charge transfer. For a constant current density higher than the limiting current density, the process rate is limited by mass transport to the electrode. In that case, oxygen evolution is the main secondary reaction occurring on the anode. In contrast, for a constant current density lower than the limiting value, the global reaction is limited by charge transfer. The initial limiting current density is calculated as follows:

$$i_{\lim}^{0} = z\ F\ k_d C^0 \tag{2}$$

where z is the number of exchanged electrons for the electrode process, F is the Faraday constant (96,487 C $mol^{-1}$), $k_d$ is the mass transfer coefficient (m $s^{-1}$) and $C^0$ is the initial concentration of the substrate (mol $m^{-3}$).

While the z number is not exactly known for an organic compound oxidized on a $PbO_2$ anode characterized by a high-oxygen overvoltage [14,15], in the case of the BDD anode, the z number is known and the concentration $C^0$ in Eq. 2 can be replaced by the initial COD expressed in mol of $O_2$ $m^{-3}$ [16] as giving in Eq. 3:

$$i_{\lim}^{0} = 4\ F\ k_d COD° \tag{3}$$

Under galvanostatic conditions, two different operating regimes are defined:

- When the applied current (I) is lower than the limiting current ($I_{lim}$), the electrolysis is controlled by the charge transfer, the current efficiency is 100% and the rate of COD removal is constant and can be written as:

$$COD(t) = COD^0\left(1-\alpha\frac{t}{\tau}\right) \tag{4}$$

In Eq. 4, α is defined as the ratio $I/I_{lim}$, t is the electrolysis time and τ is a time characteristic of the device defined as $\tau = V/(k_d A)$, where V the volume of the solution to be treated ($m^3$) and A is the electrode active area ($m^2$).

- If the applied current exceeds the limiting current ($\alpha > 1$), the process is mass transfer controlled. In this regime, COD decreases exponentially with time according to Eq. 5.

$$COD(t) = COD^0 \exp\left(-\frac{t}{\tau}\right) \tag{5}$$

Secondary reactions such as oxygen evolution take place and the instantaneous current efficiency (ICE) is lower than 100%. This parameter is calculated from COD values from Eq. (6).

$$ICE = \frac{\Delta COD_{\exp}}{\Delta COD_{th}} = 4\ F\ V\ \frac{\left[COD(t) - COD(t+\Delta t)\right]}{I\ \Delta t\ M_{O_2}} \tag{6}$$

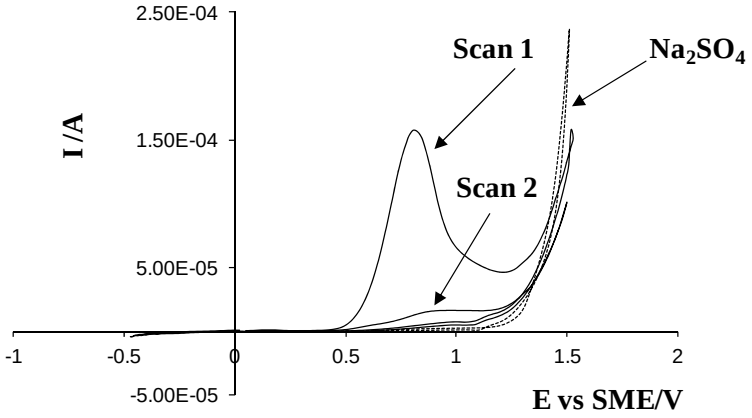


**Fig. (2).** Consecutive cyclic voltammograms (scans 1 and 2) recorded for 10 mM *m*-cresol in 0.5 M $Na_2SO_4$. The dashed curve corresponds to the electrolyte solution. Working electrode: BDD (0.196 cm²), counter electrode: Pt and reference electrode: MSE. Scan rate: 50 mV $s^{-1}$.

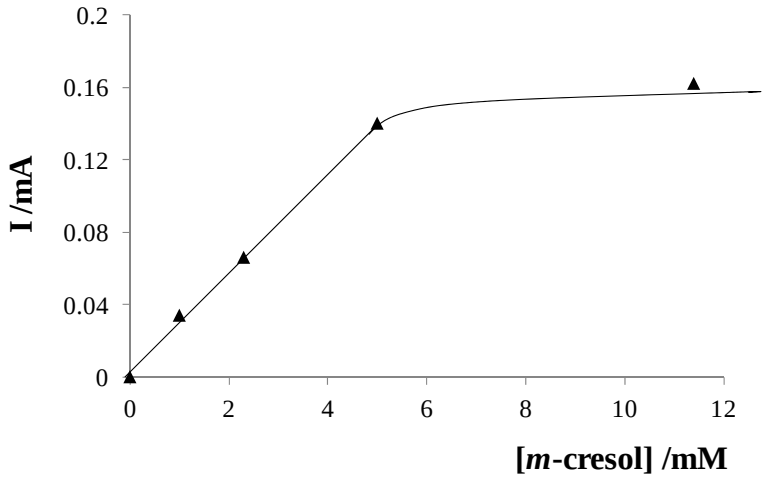


**Fig. (3).** Variation of the anodic peak current for the oxidation peak found during the first cyclic voltammetric scan as a function of *m*-cresol concentration. Working electrode: BDD (0.196 cm²), counter electrode: Pt and reference electrode: MSE. Scan rate: 50 mV $s^{-1}$.

where COD(t) and COD(t + Δt) are the concentrations of COD expressed in g $L^{-1}$ at times t and t + Δt, respectively, $M_{O_2}$ is the dioxygen molar weight (32 g $mol^{-1}$) and V is the volume of solution (L).

## 3. RESULTS AND DISCUSSION

### 3.1. Cyclic Voltammetric Study

The electrochemical behavior of *m*-cresol in sodium sulfate solution was studied by cyclic voltammetry on the BDD electrode. Fig. (**2**) shows two successive scans recorded between -0.5 and 1.5 V at 25 °C. During the first scan towards positive potentials, a well defined peak which corresponds to *m*-cresol oxidation appears before water oxidation (see dashed line). Fig. (**2**) also shows that electrode passivation occurred after the first cycle since no oxidation peak was observed in the second cycle. This behavior is due to the formation of a passive layer of polymers at the surface of the working electrode.

Various cyclic voltammograms were also carried out at different concentrations of *m*-cresol. In each case, only the first scan gave an oxidation peak at similar potentials to those shown in Fig. (**2**). After each scan, the electrode activity was restored using anodic polarisation at 2.84 V during 40 s. The variation of the anodic peak current as function of *m*-cresol concentration is shown in Fig. (**3**).

Fig. (**3**) depicts that at concentrations of *m*-cresol lower than 5 mM, the peak current varies linearly with the concentration in the solution. In contrast, at concentrations higher than 5 mM, the peak current is stabilized due to the formation of a polymer film spread on the electrode surface. This passive film blocks the electrode activity. Indeed, a visual examination of the electrode surface revealed the presence of an adherent film of polymer (see micrograph in Fig. **4**).

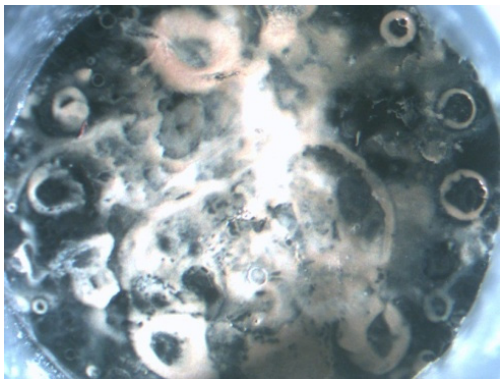

**Fig. (4).** Optical micrograph of the BDD surface after the cyclic voltammograms of Fig. (**2**). The black zone corresponds to BDD deposit and the white spots to deposited polymers.

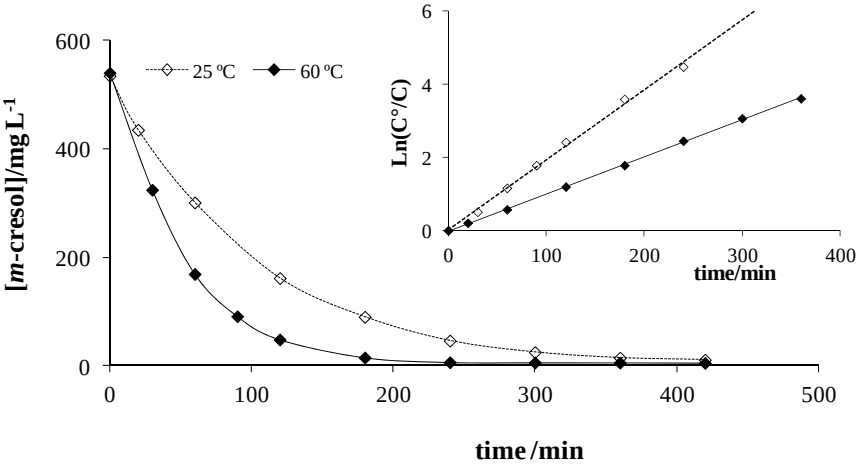


**Fig. (5).** Variation of *m*-cresol concentration during the electrolysis of 1 L of a 534 ppm *m*-cresol solution in 0.05 M $Na_2SO_4$ using a flow electrochemical cell with a BDD anode at 2.5 A, temperatures of 25 and 60 ºC and liquid flow rate of 126 L $h^{-1}$. The inset panel shows the kinetic analysis for the related experiments assuming a pseudo-first-order reaction for each temperature.

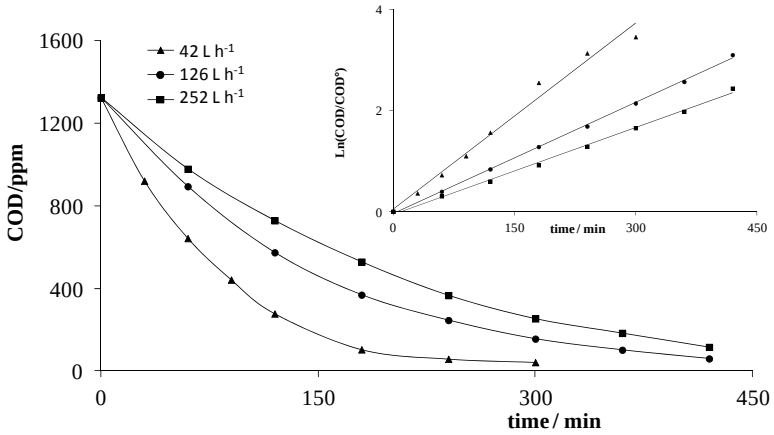


**Fig. (6).** COD abatement during the electrolysis of 1 L of a 534 ppm *m*-cresol solution in 0.05 M $Na_2SO_4$ using a flow electrochemical cell with a BDD anode at 2.5 A and 25 °C for electrolyte flow rates of 42, 126 and 252 L $h^{-1}$. The inset panel shows the kinetic analysis for the related experiments assuming a pseudo-first-order reaction for each flow rate.

Similar observations have been noted using BDD anodes in the case of phenol [17], 2-naphtol [18] and 4-chlorophenol [19]. In these papers, it is assumed that the electron transfer to the phenolic ring leads to phenoxy radicals that react to form polymeric structures by coupling reactions. This behavior could also be considered for *m*-cresol oxidation at potentials lower than those of water discharge.

### 3.2. Electrolysis in the Flow Cell Under Galvanostatic Conditions

Fig. (**5**) shows that the kinetics of the oxidation of 534 ppm of *m*-cresol in 0.05 M $Na_2SO_4$ using the flow electrochemical cell with a BDD anode is enhanced when the temperature rises. So, the compound was completely removed in 420 min at 25 ºC, but only in about 300 min at 60 ºC operating at 2.5 A and liquid flow rate of 126 L $h^{-1}$. Under these conditions, the BDD reached potentials in the water discharge region and no polymers were deposited on it.

According to our previous study [5], the above concentration decays were well-fitted to a pseudo-first-order kinetic equation. A quite similar kinetic behavior has also been described by Polcaro *et al.* [20] for the removal of phenol solutions with BDD in galvanostatic electrolysis. The inset panel of Fig. (**5**) confirms the first-order kinetics for the anodic oxidation of *m*-cresol, allowing determining the apparent kinetic constant (k) for the above temperatures. The k-value measured for the same ratio electrode surface/volume treated was $1.69\times10^{-4}$ $s^{-1}$ for 25 ºC and $3.19\times10^{-4}$ $s^{-1}$ for 60 ºC. These data allow estimating an activation energy of 15 kJ $mol^{-1}$, which is in agreement with a kinetic process limited by mass transfer [21, 22].

Fig. (**6**) highlights the influence of the flow rate on COD decay at the same operating parameters. As can be seen, the COD removal becomes more effective as the flow rate of the electrolyte is higher, indicating that the process is mass transport limited. For the electrochemical reactor, the following relation between the flow rate of the solution (u, in L $h^{-1}$) and the mass transfer coefficient ($k_d$, in m $s^{-1}$) was determined by means of the ferri/ferro redox system under the same hydrodynamic conditions [16]:

$$k_d = =2.78 \times 10^{-6}\, u^{0.38} \quad (7)$$

Note that at 25°C, for an electrolysis carried out at I = 2.5 A using a flow rate of 126 L $h^{-1}$, *m*-cresol decays in 87% at t = 200 min (Fig. **5**) while the related COD removal is smaller, close to 75% (Fig. **6**). Comparison of these *m*-cresol and COD removals confirms the almost direct conversion of the initial pollutant into carbon dioxide and water using a BDD anode, in agreement with the very few amounts of by-products reported by us previously [5]. Indeed,

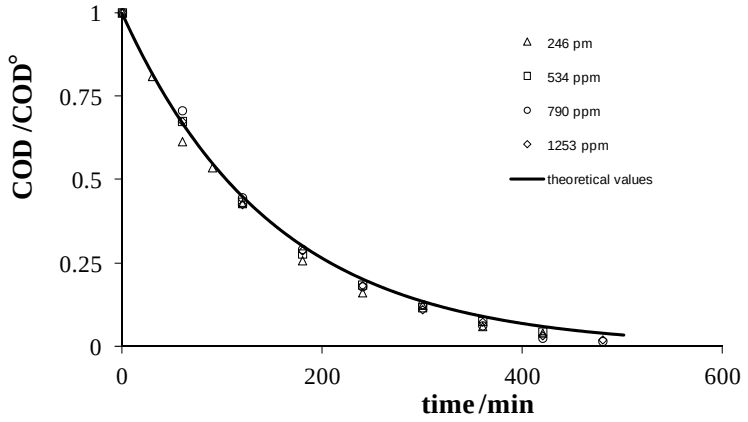


**Fig. (7).** Variation of normalized COD calculated (lines) and experimental (symbols) for the electrochemical oxidation of solutions containing *m*-cresol concentrations of 246, 534, 790 and 1253 ppm at 2.5 A, 25 º C and electrolyte flow rate of 126 L $h^{-1}$.

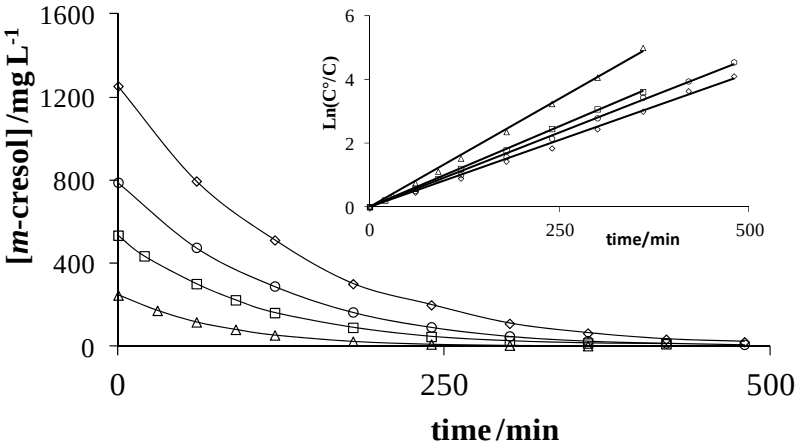


**Fig. (8).** Decay of *m*-cresol concentration for the experiments reported in Fig. **7**. The kinetic analysis for the related experiments considering a pseudo-first-order reaction for each initial concentration is depicted in the inset panel.

this study highlighted that the temporal evolution of the experimental dissolved organic carbon (DOC) obtained during galvanostatic electrolysis of a *m*-cresol solution using BDD was similar to that calculated from the *m*-cresol concentration.

Consequently, it is convenient to use the global parameter of COD and ICE to monitor the detoxification of the solution during the electrolysis (Eq 4-6).

Fig. (**7**) shows the decrease of the normalized chemical oxygen demand of *m*-cresol solutions at different initial concentrations during electrolysis carried out at 2.5 A, 25 ºC and electrolyte flow rate of 126 L $h^{-1}$. The *m*-cresol concentrations and the constant current density were chosen in such a way that the process is limited by the mass transfer to the electrode from the beginning of the electrolysis (except for *m*-cresol = 1253 ppm, I = $I_{lim}$ at 168 min). Fig. (**7**) evidences the same variation of the normalized COD with time whatever the initial concentration of *m*-cresol in the solution, reaching always overall decontamination in about 500 min. Moreover, Fig. (**7**) shows a very good agreement between the experimental and theoretical (given by Eq. 4-5) COD values. Thus, this model allows predicting the change of COD for any *m*-cresol solution. The COD variation then follows a first-order kinetics whatever the initial concentration because a *m*-cresol molecule reaching the BDD anode is almost totally mineralized, without significant formation and diffusion of by-products towards the bulk.

Fig. (**8**) shows the variation of the *m*-cresol concentration as a function of time for the same experiments of Fig. (**7**). The inset panel in Fig. (**8**) depicts that the concentration decay always verifies a pseudo-first-order kinetics and that the rate of disappearance of *m*-cresol becomes faster for smaller initial concentration. The k-values thus obtained were $2.16\times10^{-4}$, $1.69\times10^{-4}$, $1.50\times10^{-4}$ and $1.33\times10^{-4}$ $s^{-1}$ for 246, 534, 790 and 1253 ppm, respectively. Nevertheless, at a given time, increasing concentrations yield the removal of more amount of *m*-cresol.

These results can be explained as follows. The decrease in *m*-cresol concentration leads to an increasing part of the current used for water discharge by reaction (1). Thus, a higher production of oxygen bubbles occurs close to the electrode by the following sequence:

$$^{\bullet}OH + {}^{\bullet}OH \xrightarrow{k_1} H_2O_2 \quad (8)$$

$$H_2O_2 + {}^{\bullet}OH \xrightarrow{k_2} H_2O + O_2^{\bullet-} + H^+ \quad (9)$$

$$O_2^{\bullet-} + {}^{\bullet}OH \xrightarrow{k_3} O_2 + OH^- \quad (10)$$

The absolute constant rates for these reactions are $k_1 = 5.2\times10^9$ $M^{-1}s^{-1}$ [23, 24], $k_2 = 2.7\times10^7$ $M^{-1}s^{-1}$ [25, 26] and $k_3 = 10^{10}$ $M^{-1}s^{-1}$ [27, 28]. Consequently, the mass transfer coefficient increases locally. Accordingly, the kinetic constant $k = k_d A/V$ increases with decreasing *m*-cresol concentration.

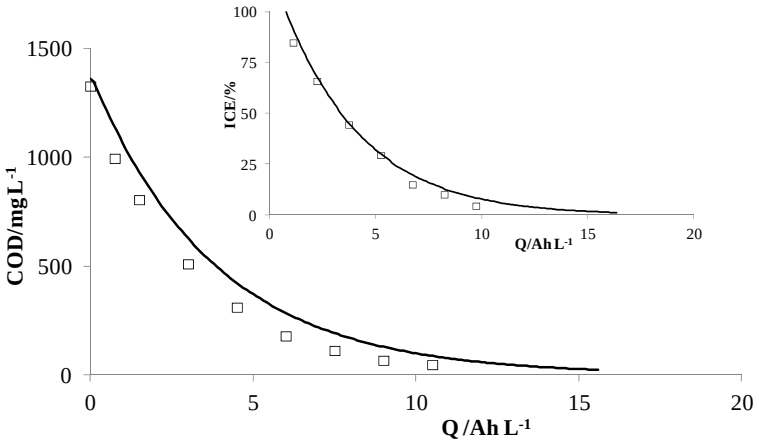


**Fig. (9).** Variation of COD and ICE (inset panel) with specific current during the electrochemical oxidation of 534 ppm *m*-cresol in 0.05 M $Na_2SO_4$ on a BDD anode. Operating conditions: I = 1.5 A, $I_{lim}$°= 1.76 A, $t_c$ = 31 min, T = 25 °C and electrolyte flow rate = 126 L $h^{-1}$. Experimental points (symbols) and theoretical variation (solid line).

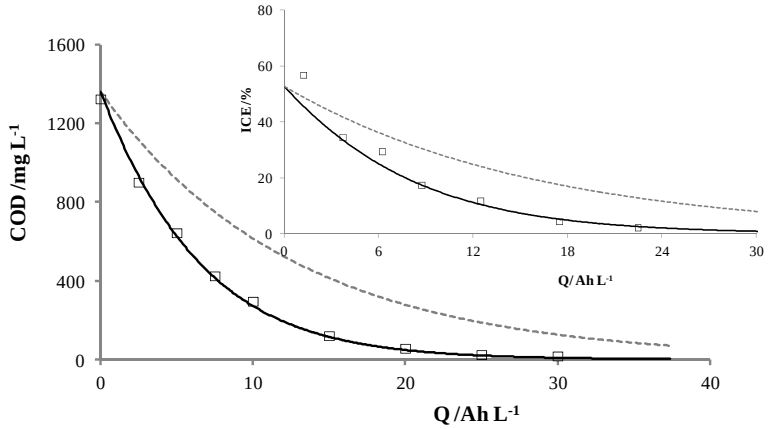


**Fig. (10).** Change of COD and ICE (inset panel) with specific current during the electrochemical oxidation of 534 ppm *m*-cresol in 0.05 M $Na_2SO_4$ $Na_2SO_4$ on a BDD anode. Operating conditions: I = 5 A, T = 25 °C and electrolyte flow rate = 126 L $h^{-1}$. Experimental points (symbols) and theoretical variation (dashed line: $k_d = k^h_d = 1.75\times10^{-5}$ m $s^{-1}$, solid line: $k_d$ corrected = $3.5\times10^{-5}$ m $s^{-1}$ (from Eq. 12)).

It is important to compare the experimental variation of COD and the theoretical values predicted by theory (Eq. 4-6) for both operating regimes:

- $I < I_{lim}^{\circ}$ (1.76 A). For this case, Fig. **9** highlights the existence of two consecutive different kinetic zones. At the beginning of the electrolysis (specific charge (Q) < 0.78 Ah $L^{-1}$, t < 31 min) and according to electron transfer control, COD varies linearly according to Eq. 4. However, at times longer than $t_c$ = 31 min, COD decreases according to an exponential decay, characteristic of a process limited by mass transfer (Eq. 5). Moreover, theoretical and experimental values for both COD and ICE (inset panel of Fig. **9**) are in quite good agreement.

- $I > I_{lim}^{\circ}$. Fig. 10 shows the variation of COD during galvanostatic electrolysis at a current widely higher than the initial limiting current. As can be seen, the experimental values are lower than those calculated from the model (Eq. 5, dashed line in Fig. **10**). A similar behavior is observed for the instantaneous current efficiency (inset panel of Fig. **10**). To explain these deviations, it can be taken into account that during the electrolysis, the depletion of organic matter leads to an increase of oxygen evolution at the anode, as pointed out above. Consequently, the rate of gas evolution close to the electrode has a great effect on mass transfer since a release of bubbles increases the mass transfer coefficient [29]. Beck [30] showed that the mass transfer coefficient $k_d$ is the sum of two contributions, the flow rate $k_d^h$ and the convection due to bubbles $k_d^b$, according to Eq. 11:

$$k_d = k_d^h + k_d^b \tag{11}$$

Nevertheless, Vogt [29] tested and proposed a more precise correlation given by Eq. 12, which takes into account the influence of the flow rate on the bubble radius before dropping out:

$$k_d = k_d^b \left[ 1 + \left( \frac{k_d^h}{k_d^b} \right)^2 \right]^{0.5} \tag{12}$$

$k_d^b$ depends on the gas flow production [29] :

$$k_d^b = \text{const} \left( \frac{\dot{V}_G}{S} \right)^m D^{0,5} \tag{13}$$

In this equation, D is the gas diffusion coefficient in liquid phase, $\dot{V}_G$ is the volumetric rate of gas evolution and S area of the flow cross section. The constant value m is function of the gas na-

ture. The average value for dioxygen in acid media is estimated to m=0.5 [30, 31].

The gas flow production, $\frac{\dot{V}_G}{S}$, is a function of the part of the applied current which produces dioxygen, $i_{O_2}$, and the molar volume of dioxygen, $V_{mol}$ :

$$\left(\frac{\dot{V}_G}{A}\right) = \frac{i_{O_2}}{n\ F}\ V_{mol} \qquad (14)$$

The constant of eq. 13 was estimated to 5.4 $10^{-3}$ with experimental data resulted from an electrolysis controlled by mass transfer à t=3h.

For Fig. (**10**), a $k_d$ value of $3.5\times10^{-5}$ m $s^{-1}$ was estimated from Eq. 12 to 14, instead of $k_d^h$ = $1.75\times10^{-5}$ m $s^{-1}$. Taking this corrected $k_d$ value, the theoretical COD and ICE decays show an excellent fitting with the experimental points, as can be seen in Fig. (**10**).

## CONCLUSIONS

The anodic oxidation of m-cresol on BDD at a potential lower than the water discharge promotes the formation of polymeric films quickly fouling the electrode. The electron transfer leads to phenoxy radicals that react to yield polymeric structures by coupling reactions. The formation of this non conductive polymer is fast and makes that the current of its anodic peak reaches a limiting value for a concentration of 5 mm. The variation of m-cresol concentration during electrolysis performed in galvanostatic mode using a flow electrochemical cell with a BDD anode corresponds to a first-order kinetics, in accordance with a process limited by mass transfer. Also, the effect of the electrolyte flow rate on the mass transfer coefficient shows that m-cresol oxidation is limited by diffusion. Experiments carried out at different temperatures allowed estimating an activation energy of 15 kj $mol^{-1}$, a rather low value which confirms a diffusion-controlled process. The COD variation evidences the excellent performance of BDD anode towards the mineralization of m-cresol. Practically all the flow of organic matter arriving at the electrode is instantaneously mineralized. The mass transfer is widely increased by oxygen evolution when the electrolysis is carried out at current higher than its limiting value.

## CONFLICT OF INTEREST

The author(s) confirm that this article content has no conflicts of interest.


## ACKNOWLEDGEMENT

Declared none.


## REFERENCES


[1] Kavitha, V.; Palanivelu, K. Destruction of cresols by Fenton oxidation process. *Water Res.*, **2005**, *39*, 3062-3072.

[2] Hatipoğlu, A.; San, N.; Çinar, Z. An experimental and theoretical investigation of the photocatalytic degradation of *meta*-cresol in $TiO_2$ suspensions: A model for the product distribution. *J. Photoch. Photobio. A*, **2004**, *165*, 119-129.

[3] Wang, K.H.; Hsieh, Y.H.; Chen, L.J. The heterogeneous photocatalytic degradation, intermediates and mineralization for the aqueous solution of cresols and nitrophenols. *J. Hazard. Mater*., **1998**, *59*, 251-260.

[4] Sivalingam, G.; Priya, M.H.; Madras, G. Kinetics of the photodegradation of substituted phenols by solution combustion synthesized $TiO_2$. *Appl. Catal. B-Environ*., **2004**, *51*, 67-76.

[5] Flox, C.; Arias, C.; Brillas, E.; Savall, A.; Groenen Serrano, K. Electrochemical incineration of cresols: A comparative study between $PbO_2$ and boron-doped diamond anodes. *Chemosphere*, **2009**, *74*, 1340-47.

[6] Brillas, E.; Sirés, I.; Oturan, M.A. Electro-Fenton process and related electrochemical technologies based on Fenton's reaction chemistry. *Chem. Rev*., **2009**, *109*, 6570-6631.

[7] Wabner, D.; Grambow, C. Reactive intermediates during oxidation of water on lead dioxide and platinum electrodes. *J. Electroanal. Chem.*, **1985**, *195(1)*, 95-108.

[8] Fleszar, B.; Płoszyńska, J. An attempt to define benzene and phenol electrochemical oxidation mechanism. *Electrochim. Acta*, **1985**, *30(1)*, 31-42.

[9] Trasatti, S. Electrocatalysis by oxides — Attempt at a unifying approach. *J. Electroanal. Chem.*, **1980**, *111(1)*, 125-131.

[10] Vitt, J.E.; Johnson, D.C. The importance of anodic discharge of $H_2O$ in anodic oxygen-transfer reactions. *J. Electrochem. Soc*., **1992,** *139*, 774-778.

[11] Kläning, U.K.; Sehested, K.; Holcman, J. Standard Gibbs free energy of formation of the hydroxyl radical in aqueous solution. Rate constants for the reaction $ClO_2^- + O_3O_3^- + ClO_2$. *J. Phys. Chem.*, **1985,** *89*, 760-763.

[12] Nava, J.L.; Núñez, F.; González, I. Electrochemical incineration of *p*-cresol and o-cresol in the filter-press-type FM01-LC electrochemical cell using BDD electrodes in sulfate media at pH 0. *Electrochim. Acta*, **2007**, *52*, 3229-3235.

[13] Mascia, M.; Vacca, A.; Polcaro, A.M.; Palmas, S.; Rodriguez Ruiz, J., Da Pozzo, A. Electrochemical treatment of phenolic waters in presence of chloride with boron-doped diamond anodes: Experimental study and mathematical model. *J. Hazard. Mat.*, **2010**, *174*, 314-322.

[14] Weiss, E.; Groenen-Serrano, K.; Savall, A.; Comninellis, Ch. A kinetic study of the electrochemical oxidation of maleic acid on boron doped diamond. *J. Appl. Electrochem.*, **2007**, *37*, 41-47.

[15] Belhadj Tahar, N.; Savall, A. Mechanistic aspects of phenol electrochemical degradation by oxidation on a Ta/$PbO_2$ anode. *J. Electrochem. Soc*., **1998**, *145*, 3427-3434.

[16] Panizza, M.; Michaud, P.A.; Cerisola, G.; Comninellis, Ch., Anodic oxidation of 2-naphthol at boron-doped diamond electrodes. *J. Electroanal. Chem.*, **2001**, *50(1-2)*, 206-214.

[17] Iniesta, J.; Michaud, P.A.; Panizza, M.; Cerisola, G.; Aldaz, A.; Comninellis, Ch. Electrochemical oxidation of phenol at boron-doped diamond electrode. *Electrochim. Acta*, **2001**, *46(23)*, 3573-3578.

[18] Panizza, M.; Cerisola, G. Influence of anode material on the electrochemical oxidation of 2-naphthol: Part 1. Cyclic voltammetry and potential step experiments. *Electrochim. Acta*, **2003**, *48*, 3491-3497.

[19] Gherardini, L.; Michaud, P.A.; Panizza, M.; Comninellis, Ch.; Vatistas, N. Electrochemical oxidation of 4-chlorophenol for wastewater treatment: Definition of normalized current efficiency. *J. Electrochem. Soc*., **2001**, *148*, D78–D82.

[20] Polcaro, A.M.; Mascia, M.; Palmas, S.; Vacca A. Electrochemical oxidation of phenolic and other organic compounds at boron doped diamond electrodes for wastewater treatment: Effect of mass transfer. *Anna. di Chim.*, **2003**, *93*, 967-976.

[21] Benson, S.W. *The Foundations of Chemical kinetics*, McGraw-Hill Book Company: New York, **1960**.

[22] Su, C.; Puls, R.W. Kinetics of trichloroethene reduction by zerovalent iron and tin: Pretreatment effect, apparent activation energy and intermediate products. *Environ. Sci. Technol.*, **1999**, *33*,163-168.

[23] Pagsberg, P.; Cristensen, H.; Rabani, J.; Nilsson, G.; Fenger, J.; Nielsen, S.O. Far-ultraviolet spectra of hydrogen and hydroxyl radicals from pulse radiolysis of aqueous solutions. Direct measurement of the rate of H+H. *J. Phys. Chem*., **1969**, *73*, 1029-1038.

[24] Thomas, J. K. Rates of reaction of the hydroxyl radical. *Trans. Faraday Soc*., **1965,** *61*, 702-707.

[25] Buxton, G.V.; Greenstock, C.L.; Helman, W. P.; Ross, A.B. Critical review of rate constants for reactions of hydrated electrons, hydrogen atoms and hydroxyl radicals, (OH, $O2^-$) in aqueous solution. *J. Phys. Chem. Ref. Data*, **1988**, 17, 513-886.

[26] Christensen, H.; Sehested, K.; Corfitzen, H. Reactions of hydroxyl radicals with hydrogen peroxide at ambient and elevated temperatures. *J. Phys. Chem.*, **1982**, *86*,1588-1590.

[27] Elliot, A.J.; Buxton, G.V. Temperature dependence of the reactions OH + $O_2^-$ and OH + $HO_2$ in water up to 200 °C. *J. Chem. Soc., Faraday Trans*., **1992**, *88*, 2465-2470.

[28] Christensen, H.; Sehested, K.; Bjergbakke, E. Temperature dependence of the reactions OH + $O_2^-$ and OH + $HO_2$ in water up to 200 °C. *Water Chem. Nucl. React. Syst.*, **1989**, *5*, 141-144.

[29] Vogt H. Mass transfer at gas involving electrodes with superposition of hydrodynamic flow. *Electrochim. Acta*, **1978**, *23*, 203-205.

[30] Beck T.R.. A contribution to the theory of electrolytic chlorate formation. *J. Electrochem. Soc.*, **1969**, *116(7)*, 1038-1041.

[31] Janssen, L.J.J.; Hoogland, J.G.. The effect of electrolytically evolved gas bubbles on the thickness of the diffusion layer. *Electrochim. Acta*, **1970**, *15*, 1013-1023.